Observational upper limits for low-l solar g modes

C.Fröhlich[1], T.Appourchaux[2], B.Andersen[3], G.Berthomieu[4], W.J.Chaplin[2], Y.Elsworth[5], W.Finsterle[1], D.O.Gough[6], J.T.Hoeksema[7], G.R.Isaak[5], A.G.Kosovichev[7], J.Provost[7], P.H.Scherrer[7], T.Sekii[6], T.Toutain[4]

ABSTRACT

Observations from the Michelson Doppler Imager (SOI/MDI) and Variability of solar IRradiance and Gravity Oscillations (VIRGO) on the Solar and Heliospheric Observatory (SOHO) and from the Birmingham Solar Oscillation Network (BiSON) have been used in a concerted effort to search for solar gravity oscillations. All spectra are dominated by solar noise in the frequency region where g modes are expected. Several methods have been used to extract the g-mode signal, such as correlation of signals during different time intervals from the same instrument to search for long-term coherent signals, correlation of signals of different instruments to reduce non-coherent solar signals, correlation of signals with different spatial masks of the same instrument, linear filtering of data from different colours to enhance signals buried in the noise. The detection limit is set by the semi-coherent signal caused by the temporal evolution and motion, e.g. by rotation of superficial structures. Although we can not identify any g-mode signature, we can estimate an upper limit for their amplitude: in the frequency range from xxx-yyy μHz it is below 1 mms^{-1} in velocity, or below 0.1 parts-per-million in intensity. This corresponds to a peak-to-peak vertical displacement of $\delta r/r_\odot = vvv \cdot 10^{-9}$.

Subject headings: sun, helioseismology, etc

---

[1]Physikalisch-Meteorologisches Observatorium Davos, World Radiation Center, CH-7260 Davos Dorf, Switzerland

[2]Space Science Department, P.O.Box 299, NL-2200AG Noordwijk, The Netherlands

[3]Norwegian Space Centre, N-0212 Oslo, Norway

[4]Département Cassini, URA CNRS 1362, Observatoire de la Côte d'Azur, F-06304 Nice, France

[5]School of Physics and Astronomy, University of Birmingham, Edgbaston, Birmingham, B15 2TT, United Kingdom

[6]Institute of Astronomy, University of Cambridge, Cambridge CB3 OHA, United Kingdom

[7]W.W.Hansen Experimental Physics Laboratory, Stanford University, Stanford, CA 94305, USA

1. Introduction

Helioseismology as a diagnostic tool has been highly successful over the past two decades. The most recent results obtained are summarized by Christensen-Dalsgaard (1998); additional references can be found in the proceedings of the SOHO6 Workshop which contain also this summary article. Even though the study of p-mode frequencies have revealed a wealth of information about the internal structure of the Sun. The p-mode properties, however, imply that only little information about the solar core can be deduced. To obtain detailed information about the physical structure and the dynamics of the energy generating core the identification and classification of internal gravity modes is needed. Thus the search for solar gravity oscillations has been the goal of several investigations, especially on SOHO with the most precise data.

The first claims of g-mode detection were reported by Kotov et al. (1978), Scherrer et al. (1979) and by Delache & Scherrer (1983). The lowest g-mode amplitude was about 300 mm/s with a 1-σ noise of about 200 mm/s in the 45-105 μHz range (See Scherrer 1984). These detections have never been confirmed later using either velocity or intensity data (for a review see Fröhlich & Andersen 1995). Another claim was reported by Thomson et al. (1995) using solar wind data from Ulysses. Besides the fact that they had no explanation for the propagation of g-mode signal into the solar wind, this claim has in the mean time been questioned as a result of further data analysis (Hoogeveen & Riley 1998).

There are numerous helioseismic experiments that are yet to discover g modes. They are being operated either from space such as GOLF[1], VIRGO[2] and SOI/MDI [3]; or from the ground such as BiSON[4], GONG[5] and IRIS[6]. One year after the launch of SOHO[7], it became clear that the g modes could not be detected by a single instrument.

Thus, a g-mode search group was formed in March 1997 from the VIRGO, MDI and BISON teams. The objective of this working group, the *Phoebus* group, was to join forces not only to improve the way data can be analyzed by former and newly developed methods, but also by using combined sets of data to enhance the information content by cross correlations. The data from the different instruments are freely shared. Teleconferences are held bi-monthly for speeding up data preparation, discussing scientific issues and 'new findings', and for improving communication. The Phoebus group had two workshops held in November 1997 and October 1998. The purpose of the

---

[1]Global Oscillations at Low Frequency

[2]Variability of solar IRradiance and Gravity Oscillations

[3]Solar Oscillation Investigation / Michelson Doppler Imager

[4]Birmingham Solar Oscillation Network

[5]Global Oscillation Network Group

[6]Investigation on the Rotation and Interior of the Sun

[7]Solar and Heliospheric Observatory, a ESA/NASA Mission

workshops is not only to have lively discussions but also to achieve some useful work. This is done either by sitting together computing and/or calculating what was previously discussed. In this sense, they are real *work*shop.

In this paper, we report on the findings of the *Phoebus* group. We have not found any g modes but we can put some upper limit on what we can detect either in velocity or in intensity. We describe the data utilized, and derive upper limits for the g-mode amplitude obtained with various methods.

2. Observations

2.1. SOI/MDI data

The SOI/MDI data used for the purpose of this paper are the LOI-proxy velocities (Hoeksema et al. 1998). They consist in a set of calibrated velocites measured in the 180 bins of the LOI-proxy "instrument" over a period of 784 days (from May 1, 1996 to June 23, 1998). The sampling interval is 1 minute and the duty cycle is better than 98%. No gap-filling technique was used for these data.

The timeseries were built for each (l,m) mode using optimal masks (Toutain & Kosovichev 1998) in order to minimize the mode blending in the p-mode frequency range. Hence, it could happen that these timeseries do not reflect the best signal-to-noise ratio achievable with the data in the g-mode frequency range. A straight comparison with timeseries built with spherical-harmonic masks shows that the noise level achievable can be smaller by up to 30%.

2.2. VIRGO data

The VIRGO data are managed and processed at the VIRGO Data Centre (VDC) which is located at the IAC in Tenerife. The raw data that arrive at the VDC from the Operation Facility of SOHO are known as level-0 data. Level-1 data are those that have been converted to physical units; they include the calibrations and contain all the corrections known *a priori* for instrument-related effects, such as the influence of temperature variation. The signals are also reduced to 1 AU distance and to zero radial velocity. The processing is based on the algorithms developed and tested by the CoI responsible for the instrument concerned. For the analysis presented here detrended level-1 are used.

A detailed description of the data acquisition, operation and the instruments can be found in Fröhlich et al. 1995. The data from PMO6V, SPM and LOI used in the present analysis are described in the

2.3. VIRGO data

The VIRGO data are managed and processed at the VIRGO Data Centre (VDC) which is located at the IAC in Tenerife. The raw data that arrive at the VDC from the Operation Facility of SOHO are known as level-0 data. Level-1 data are those that have been converted to physical units; they include the calibrations and contain all the corrections known *a priori* for instrument-related effects, such as the influence of temperature variation. The signals are also reduced to 1 AU distance and to zero radial velocity. The processing is based on the algorithms developed and tested by the CoI responsible for the instrument concerned. For the analysis presented here detrended level-1 are used.

A detailed description of the data acquisition, operation and the instruments can be found in Fröhlich et al. 1995. The data from PMO6V, SPM and LOI used in the present analysis are described in the following Sections.

2.3.1. Total and spectral irradiance

Two radiometers PMO6V and DIARAD measure the total irradiance and the sunphotometer (SPM) measure the spectral irradiance in three 5 nm wide spectral bands in the red (862 nm), green (500 nm) and blue (402 nm) part. Their performance has been described in Anklin et al. 1998. For the present study the data from the PMO6V radiometer and the SPM are used. The sampling interval is 1 min with a duty cycle of more than 95 % for the SPM and 33% for the radiometer.

The total length of the time series used is 853 days, starting 22 February 1996. The data fill factors are 94.1 % for PMO6V, and 92.7 %, 95.2 %, and 95.8 % for the red, green, and blue channel respectively. Because the interference filter of the SPM suffer from substantial degradation and to a lesser extent also the radiometer, proper detrending of the time series is essential. A running mean of triangular shape of two days base width is used to detrend the time series and to calculate the relative variations. The solar noise amplitude levels between $100 \ldots 500 \mu$Hz are constant and about 0.16 ppm, 0.09 ppm, 0.18 ppm, and 0.32 ppm for the total, red, green, and blue channels, respectively. Above 500 μHz the noise amplitude decreases with $\approx \nu^{-2/3}$.

2.3.2. VIRGO/LOI data

The performance of the Luminosity Oscillation Imager (LOI) can be found in Appourchaux et al. 1997. Hereafter, we briefly discuss the data reduction. The level-0 data are first converted from counts to engineering values using the calibration performed on ground. The 16 pixels are then converted to 1 AU radiance using the SOHO-Sun distance. The correction takes into account the real shape of the pixels, the limb darkening at 500 nm (Neckel & Labs 1994), and the in-flight

size of the solar image at 1 AU. The precision of the correction is for all the scientific pixels better than 0.1 %. The pixels are also converted to zero radial velocity. The 16 pixels are corrected from the variations of pixel illumination using the attitude data of the spacecraft.

At this stage the signals from the 12 scientific pixels are ready for extracting the p modes. First, each pixel is detrended using a triangle smoothing with a full width of 1 day, and then the residuals are converted to relative values. For extracting a given degree, the 12 pixels are combined using spherical harmonic filters (Appourchaux & Andersen 1990, Appourchaux et al. 1998b). Since these filters are complex they allow to separate each m in a l, n multiplet. The leakage properties of such filters is well known (Appourchaux et al. 1998b). The filters are computed weekly using the real size of the solar image, which was calibrated in flight, and the orientation of the Sun (the B angle, P is maintained zero by the spacecraft orientation). The filters are averaged over the observation time to produce a single filter which is applied to the pixel time series to produce the (l, m) signal. The time series utilized here starts on March 27th, 1996 and ends on June 24th, 1998 (819 days) with a 99% data fill.

2.4. BiSON data

Unlike those derived from the SOHO instruments, a BiSON frequency spectrum must be generated from an appropriate (coherent) combination of data collected by six network instruments. The comparative quality of the data will inevitably vary, with some stations better suited to the study of low-frequency phenomena than others. In order to maximize one's ability to detect long-period solar p and g modes, data selection criteria are required that take into account the quality of the observations made at each site over the frequency range of interest. The need to maximize the duty cycle of the network implies that data should be used, where available, from a given station. However, there is a trade-off between: (i) the introduction of these data to the final time series; and (ii) the possibility that – if they are of poor quality – their use may drive up the noise power level of the combined network set to such an extent that this negates the apparent advantage of using the data in the first place.

We have expressed the above in a quantitative manner (Chaplin 1999, in preparation) so that this essentially reduces to a non-linear, multi-parameter minimization problem. The resulting procedure was then applied in order to select data – collected over the period 1994 May 16 through 1997 Jan 10 (971 days) – to optimize the combined BiSON time series for the frequency range $200 \leq \nu \leq 1000\,\mu$Hz. The data fill is about 61%. [At frequencies below $\sim 200\,\mu$Hz, contamination by window-function-related artifacts becomes severe; however, this is not of serious concern since the strongest g modes (i.e., those most-likely to be detected first) are expected to be found at frequencies above this.

2.5. GONG data

The GONG instrument observes solar radial velocities in the NiI 676.8 nm using a Michelson interferometer, and a set of 6 stations place around the globe (Leibacher et al, 1996). The data reduction has been described by Hill et al. (1996). Similarly to the MDI and LOI instrument, spherical harmonics filters are applied to the pixel time series to extract the mode signal. For low degree modes, the leakage properties of the GONG instrument are also well understood (Appourchaux et al. 1998b).

The time series available here are almost 3.5 years of data starting May 24, 1995 to September 29, 1998 (1224 days). The data fill is 84%. During the reduction a difference filter is applied to the time series. Thus, we corrected the power by dividing the GONG spectra by the following transfer function:

$$f(\nu) = 4\sin^2(\pi\nu\Delta t) \tag{1}$$

where ν is the frequency and Δt is the sampling time (=60 s).

3. Upper limit for g-mode amplitude

3.1. Scaling of frequency spectra

All frequency spectra presented in this paper have been divided by the fractional duty cycle $\mathcal{F}$ such that, for a time-series of length N samples:

- A (commensurate) sine wave of amplitude A will correspond to a power of $\mathcal{F}A^2$ in the frequency domain (i.e., $\sqrt{\mathcal{F}}A$ in amplitude).
- A white-noise (Gaussian) source with a zero mean, characterized by a sample standard deviation of σ, will give a mean power level in the frequency domain of σ^2/N.

3.2. From full disk data alone

In this section we use a simple statistical argument for detecting g modes (Appourchaux 1998). The statistical property of the power spectra of full-disk integrated instruments is known to have a χ^2 distribution with 2 degrees of freedom. For imaging instruments, this is slightly more complicated due to the correlation between the $2l+1$ signals leading to a multinormal distribution (Appourchaux et al. 1998b). For full-disk instruments the relative level in a power spectrum (s_{det}) for which a peak due to noise has a probability of (p_{det}) to appear in a given frequency bandwidth (Δ_{det}) can easily be determined. It depends upon the observing time (T) because the number of

frequency bins in the bandwidth will increase with time and we have

$$s_{det} = \log(T) + \log(\Delta_{det}) - \log(p_{det}) \tag{2}$$

where the units of T are 10^6 sec and of Δ_{det} in μHz. For e.g. a 70-μHz band, a one year observing time and a 0.1 probability level the detection level corresponds to 10 σ. The 70-μHz band approximately corresponds to the distance between 2 p modes; the band was slightly ajusted to get the number 10! We used these modes as a test bed for the detection criteria. All levels hereafter are computed according to this baseline taking into account the observing time such that s_{det} can be simply written as:

$$s_{det} = 10 + \log(T_y) \tag{3}$$

where T_y is now the observing time in years.

3.2.1. BiSON

Figure 1 shows the amplitude spectrum generated from the coherent combination of those BiSON data that met the quality-selection criteria during the 971-day period. The fractional duty cycle of the time series is $\mathcal{F} \sim 61$ per cent. The solid line indicates the 10-per-cent threshold level as a function of frequency. As indicated in Section 3.1, the ordinate is scaled such that a commensurate sine wave with amplitude A will give a peak of amplitude $\sqrt{\mathcal{F}}A$ in the frequency domain; therefore, the amplitudes of potential candidate peaks in Fig. 1 must be multiplied by $1/\sqrt{\mathcal{F}}$ in order to recover the equivalent sine-wave amplitude. We indicate this level by the dashed line on the plot.

Taking the above into account, we estimate that the upper (detectable) limit to the amplitude, A, of any modes present decreases from about ~ 15 to $\sim 10\,\mathrm{mm\,s^{-1}}$ over the range ~ 200 to $\sim 300\,\mu$Hz. (Were the duty cycle of the time series to have been 100 per cent – with data of similar quality filling the gaps – the thresholds would have been reduced to about ~ 12 and $\sim 8\,\mathrm{mm\,s^{-1}}$ respectively.)

Of the most prominent low-frequency peaks in the BiSON spectrum, none match, to within a reasonable tolerance, the modeled frequencies (model 'S') of Christensen-Dalsgaard et al. (1996). For example, the peak at $527.31\,\mu$Hz lies some $\sim 8.6\,\mu$Hz from the nearest predicted frequency (of the $l = 0$, $n = 3$ p mode). Below $200\,\mu$Hz, the most-striking peaks are readily identifiable as daily harmonics.

In an effort to reveal the presence of rotationally split modal peaks, we applied a pattern-recognition procedure similar to that used on the imaged data (as the "collapsoimage"). An "overlapoimage" is made by suitably shifting and co-adding the full-disc spectrum an appropriate number of times, over some chosen range in frequency; the range is then incremented and the raster dimension built up. Each diagram in principle reveals a pattern made simultaneously from

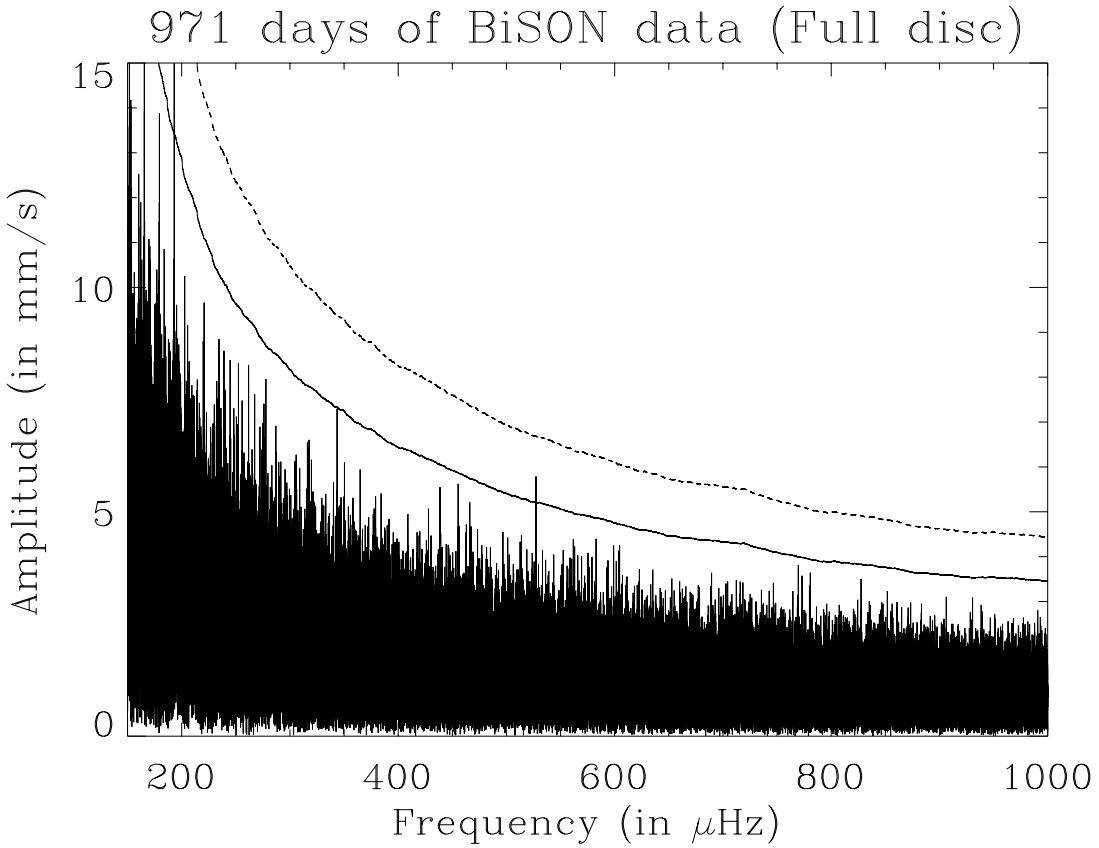

Fig. 1.— BiSON amplitude spectrum corrected from the filling factor. The continuous line gives the 0.1 probability limit that a peak be due to noise in a 70 μHz bandwidth. In the power spectrum, this level is about 11 σ, e.g. about $\sqrt{11}$ in the amplitude spectrum.

all visible m components. We found no evidence for the presence of any mode multiplets when we applied this technique to the BiSON spectrum.

3.2.2. SPM

Various detection techniques have been used to seek g mode and low order p mode signatures in the full disk irradiance spectra from VIRGO. Multi-variate Regression Analysis (cf. sect. 3.4), Time-Frequency Analysis and a Statistical Survey turned out to be the most promising techniques. Their detection probabilities were tested on a set of ten artificial modes, which were inserted into the time series of the three SPM channels (spectral irradiance) and the PMO6 radiometer (total irradiance). For a signal-to-noise ratio of 3, with the noise level defined as the running mean amplitude over 1000 frequency bins, the detection probability is $30 \ldots 40$ %. In the considered frequency range (1000-100 μHz) the corresponding mode amplitudes are 0.3 to 0.5 ppm for PMO6, 0.2 to 0.3 ppm for SPM Red, 0.4 to 0.6 ppm for SPM Green and 0.6 to 0.9 ppm for SPM Blue channels. To enable interference with the noise, the artificial modes were introduced as sine waves in the time series rather than as peaks in the Fourier spectra. It turned out that the detectability of a mode with a given signal-to-noise ratio may vary by a factor of 2 depending on the characteristics of the noise in its immediate neighborhood.

3.3. From resolved data alone

Various pattern techniques have been used for detecting g modes. All the pattern techniques assume that the g modes are splitted by rotation and/or that their frequencies are derived from an asymptotic formula (Fröhlich & Andersen 1995; Fröhlich & Delache 1984). We have devised a new pattern technique for detecting g modes: *the collapsogramme*. Each m spectrum is shifted from the $m = 0$ spectrum by $m\Omega$ (where Ω represents the splitting of the mode), then each spectrum is normalized by an estimate of the variance of the spectrum in a narrow frequency band, the $2l+1$ spectra (shifted and normalized) are added together; the final spectrum is normalized by the number of spectra $(2l + 1)$ for comparison with single power spectra. The advantage of this technique is that it gets rid of the instrumental harmonics (invariant), and produces a spectrum with a well defined statistics (nearly a χ^2 with $4l + 2$ d.o.f.). The disadvantage is that the g-mode splitting varies faster with frequency than for the p modes; the technique should be restricted to frequency band where the splitting varies slowly. Lower-frequency p modes can be detected showing the efficiency of the technique (Appourchaux et al. 1998a, Rabello-Soares & Appourchaux 1999).

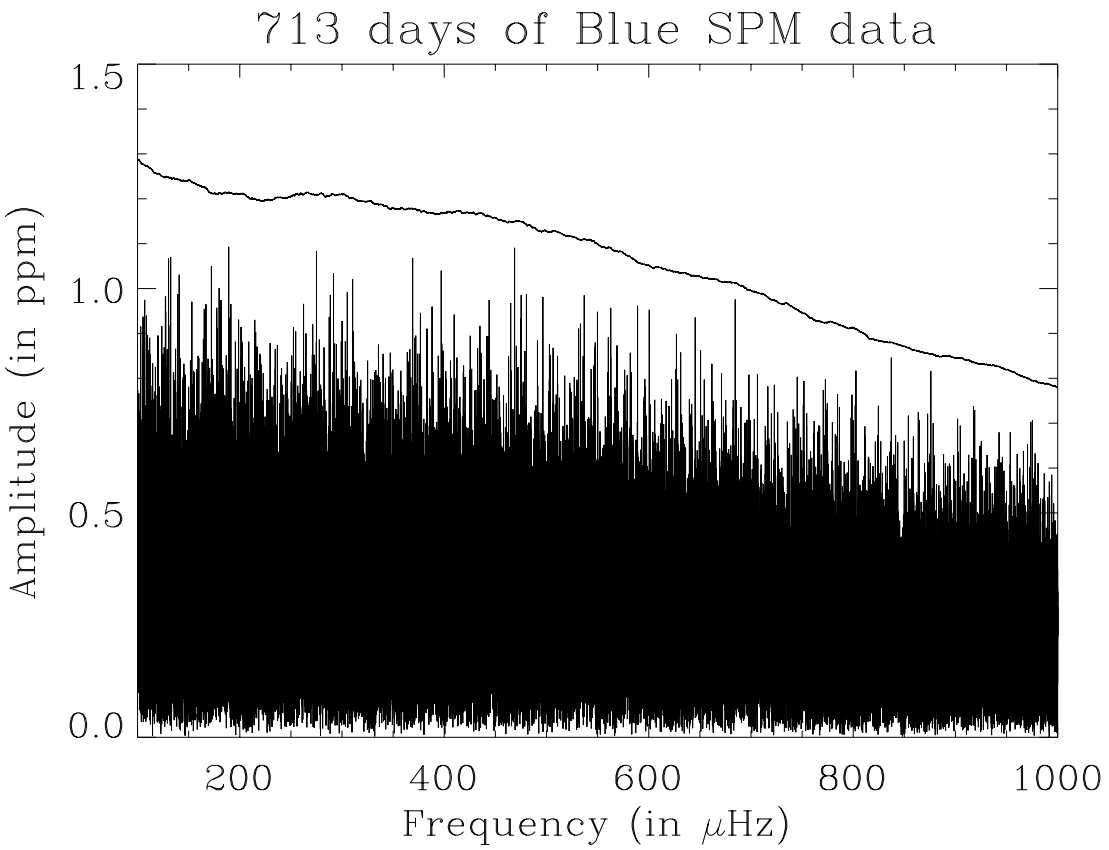

Fig. 2.— SPM amplitude spectra for the Blue channel. The continuous line gives the 0.1 probability limit that a peak be due to noise in a 70 μHz bandwidth. In the power spectrum, this level is about 10.7 σ, e.g. about $\sqrt{10.7}$ in the amplitude spectrum.

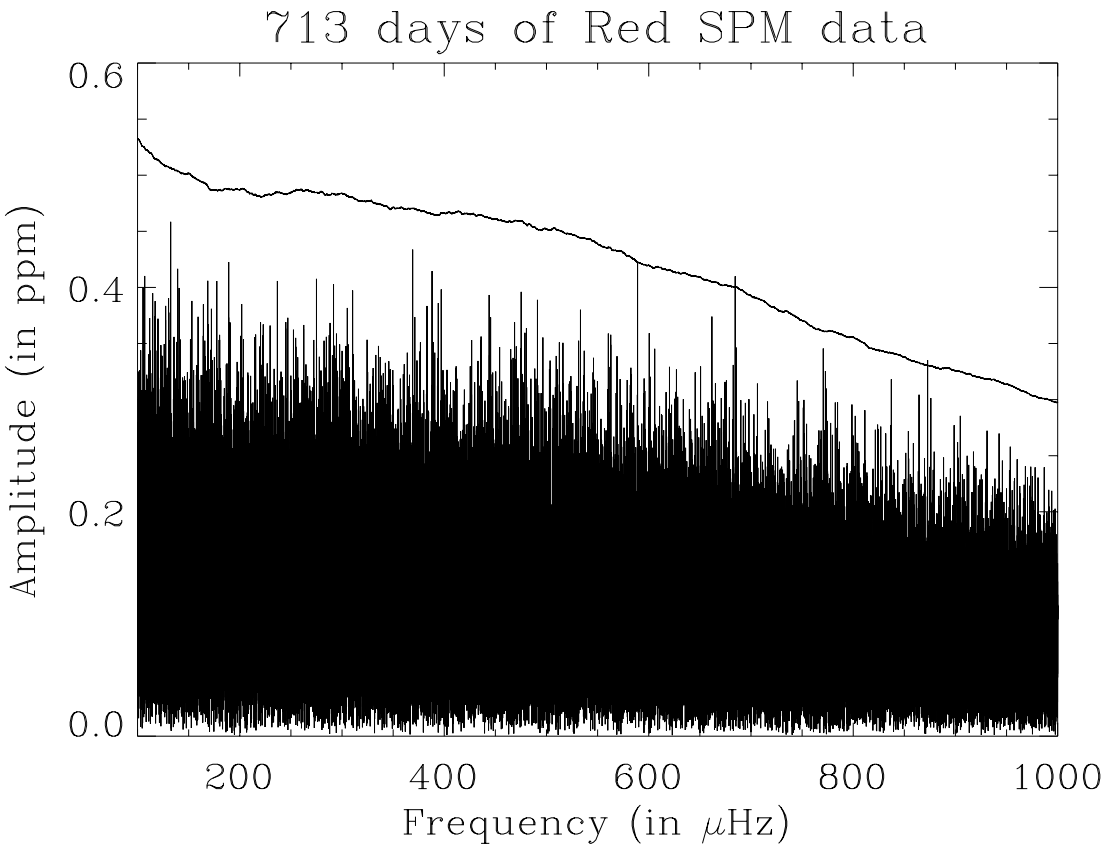

Fig. 3.— SPM amplitude spectra for the Red channel. The continuous line gives the 0.1 probability limit that a peak be due to noise in a 70 μHz bandwidth. In the power spectrum, this level is about 10.7 σ, e.g. about $\sqrt{10.7}$ in the amplitude spectrum

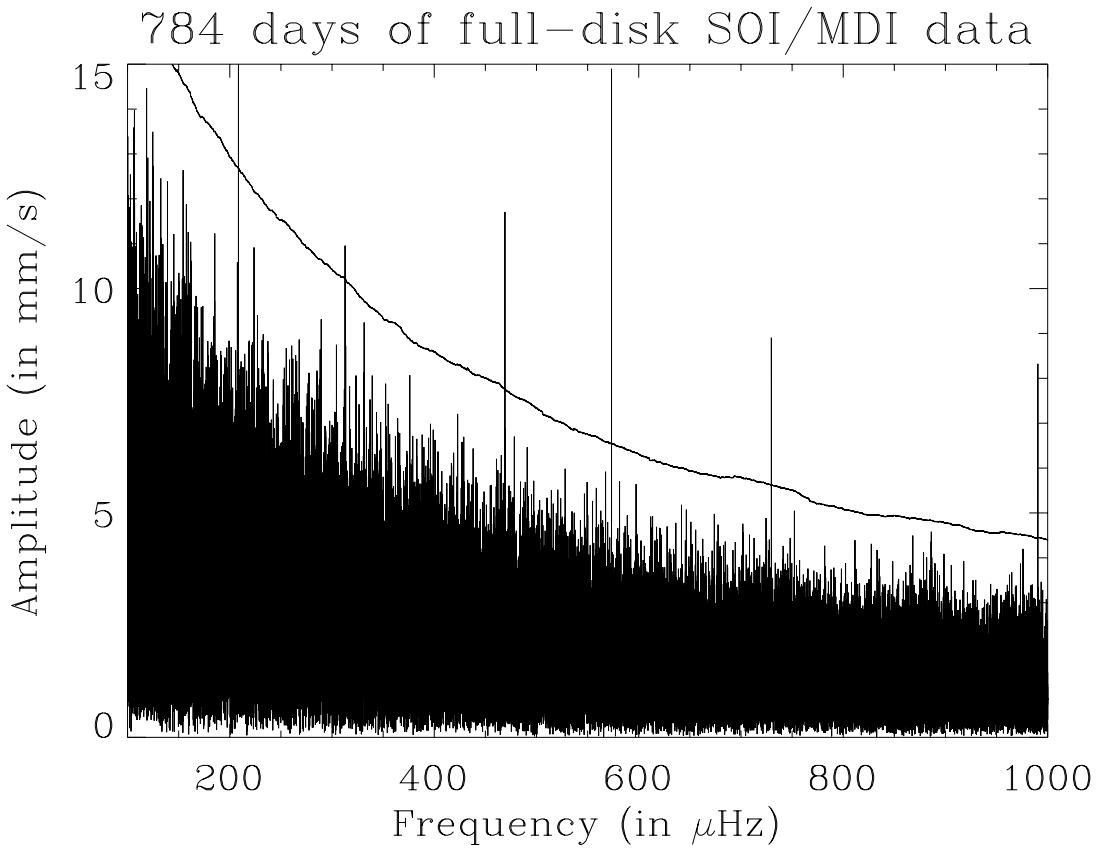

Fig. 4.— SOI/MDI amplitude spectra for $l = 0$, $m = 0$. The continuous line gives the 0.1 probability limit that a peak be due to noise in a 70 μHz bandwidth. In the power spectrum, this level is about 10.8 σ, e.g. about $\sqrt{10.8}$ in the amplitude spectrum. Most of hte peaks above the detection limit are due to harmonics of 52 μHz related to timing interferences within MDI.

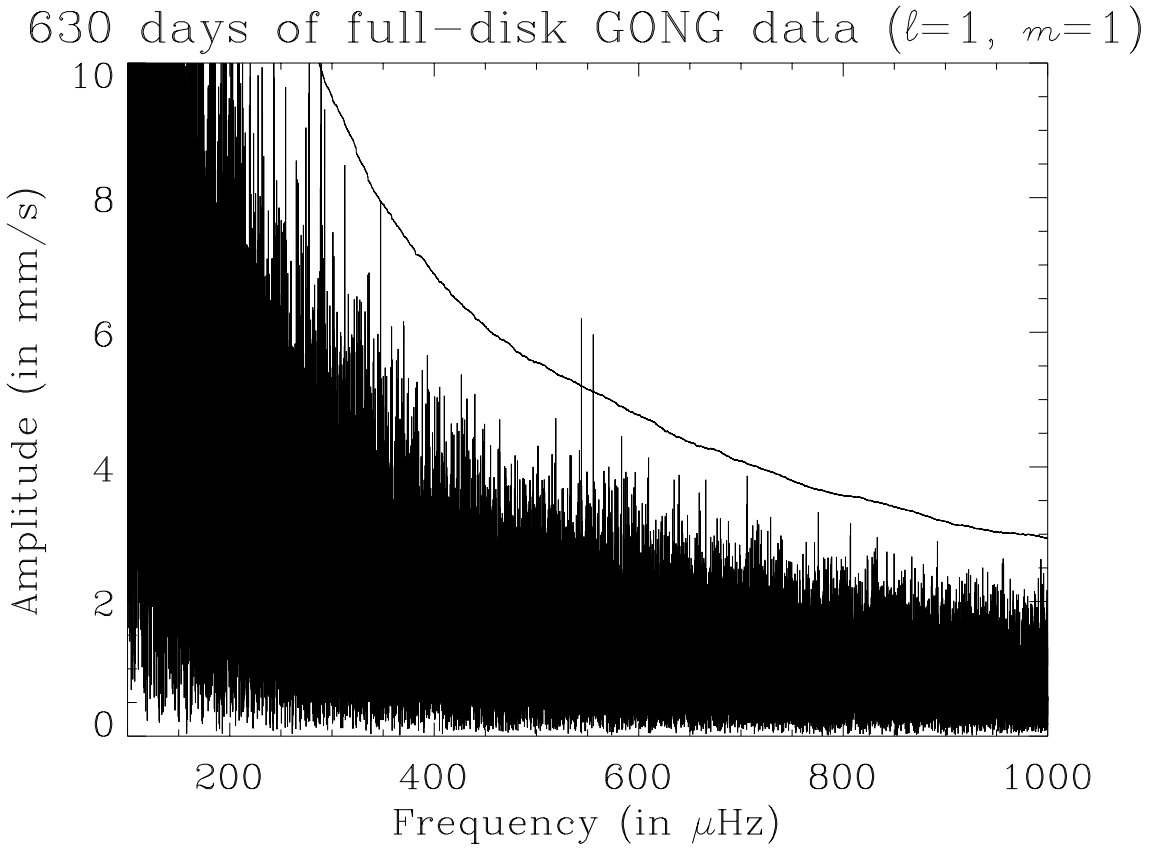

Fig. 5.— GONG amplitude spectra for $l = 0$, $m = 0$. The continuous line gives the 0.1 probability limit that a peak be due to noise in a 70 μHz bandwidth. In the power spectrum, this level is about 11.2 σ, e.g. about $\sqrt{11.2}$ in the amplitude spectrum.

3.3.1. LOI

Figure 6 and 7 shows the collapsogrammes obtained for $l = 1, 2$. **Obviously some more text is needed here: noise level, gain over full disk**

3.3.2. SOI/MDI

Figure 8 and 9 shows the collapsogrammes obtained for $l = 1, 2$. **Obviously some more text is needed here: noise level, gain over full disk**

3.3.3. GONG

Figure **??** and **??** shows the collapsogrammes obtained for $l = 1, 2$. **Obviously some more text is needed here: noise level, gain over full disk**

3.4. From combining data sets

Multivariate spectral regression analysis ($MSRA$) can be used to determine how much of the variance in one time series can be explained by the variance of other simultaneous time series. It is explaining the *dependent* component $Y(t)$ of a multivariate vector process by linearly filtering its *independent* components $\mathbf{X}(t)$, as

$$Y(t) = \mathbf{L}(\mathbf{X}(t)) + \eta(t), \tag{4}$$

where $Y(t)$ is the 1-dimensional process of the dependent component and $\mathbf{X}(t)$ is the $(p \times 1)$-vector process of the independent components. $\mathbf{L}$ is a multivariate linear filter with unknown $(1 \times p)$-dimensional transfer functions $\mathbf{B}(\lambda)$ which transform the coherent part of the independent time series into the coherent part of the dependent series. $\eta(t)$ is the unobservable 1-dimensional residual (error) process which is not correlated with $\mathbf{X}(t)$.

The extent of deviation of $Y(t)$ from a linear function of $\mathbf{X}(t)$ is measured by the unknown *spectral density function* $f^{\eta}(\lambda) = \frac{dF^{\eta}(\lambda)}{d\lambda}$, where $F^{\eta}(\lambda)$ is the spectral distribution of $\eta(t)$. $f^{\eta}(\lambda)$ and the *transfer function* are the principal parameters of interest. $\mathbf{B}(\lambda)$ indicates how the various inputs are parcelled to the output series. They are determined by minimizing the expectation value $E\eta^2(t)$. The transfer function of $\mathbf{B}$ and the spectral density function of $\eta(t)$ can be calculated according to

$$\mathbf{B}(\lambda) = \mathbf{f}^{Y,X}(\lambda)\mathbf{f}^{X}(\lambda)^{-1} \tag{5}$$

and

$$f^{\eta}(\lambda) = f^{Y}(\lambda) - \mathbf{f}^{Y,X}(\lambda)\mathbf{f}^{X}(\lambda)^{-1}\mathbf{f}^{X,Y}(\lambda),$$

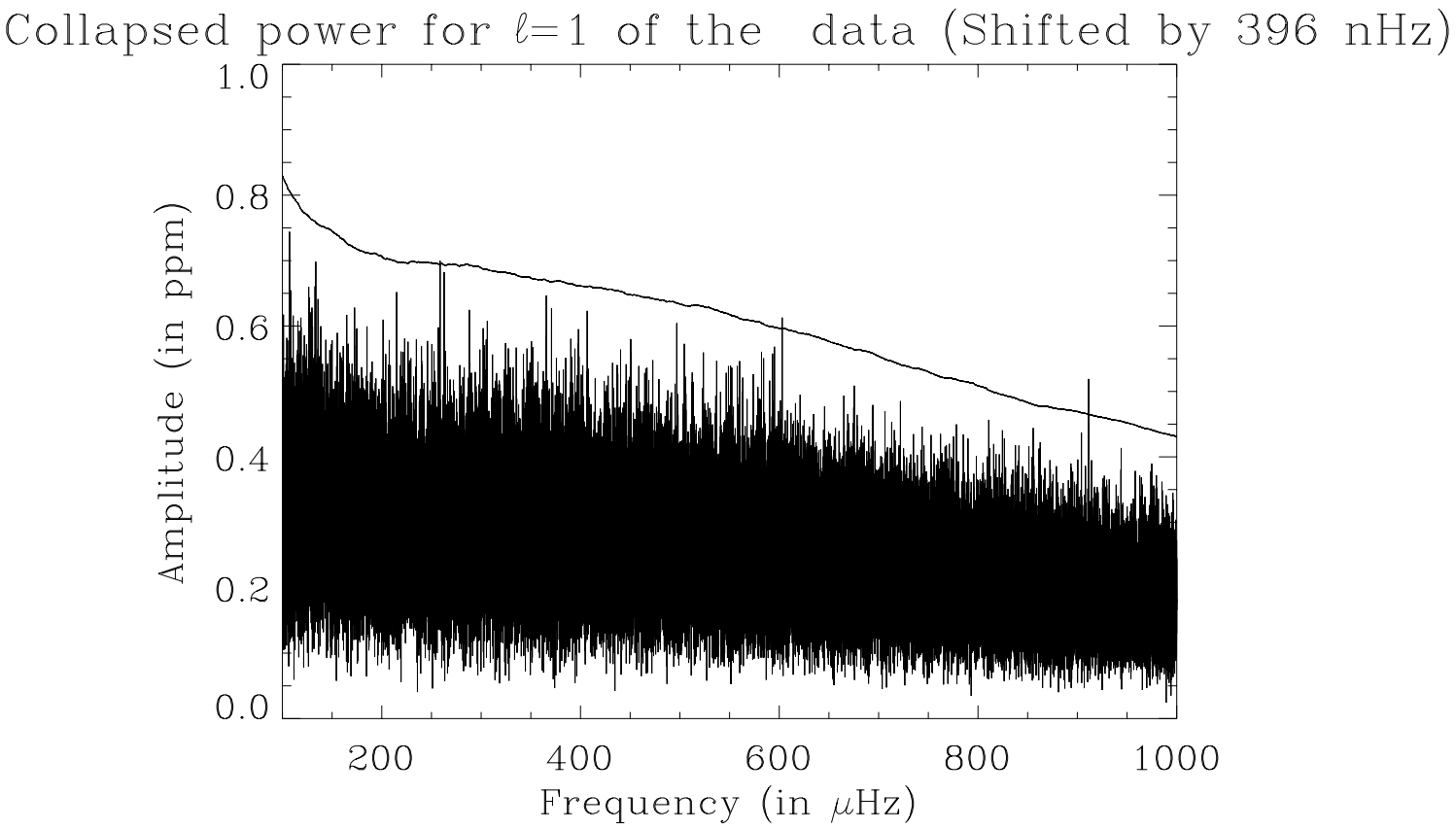

Fig. 6.— LOI collapsed spectra for $l = 1$. The continuous line gives the 0.1 probability limit that a peak be due to noise in a 70 μHz bandwidth. In the power spectrum, this level is about 10.5 σ, e.g. about $\sqrt{10.5}$ in the amplitude spectrum; this level is to be compared with the level of 10.8 that would have been obtained with a single power spectrum

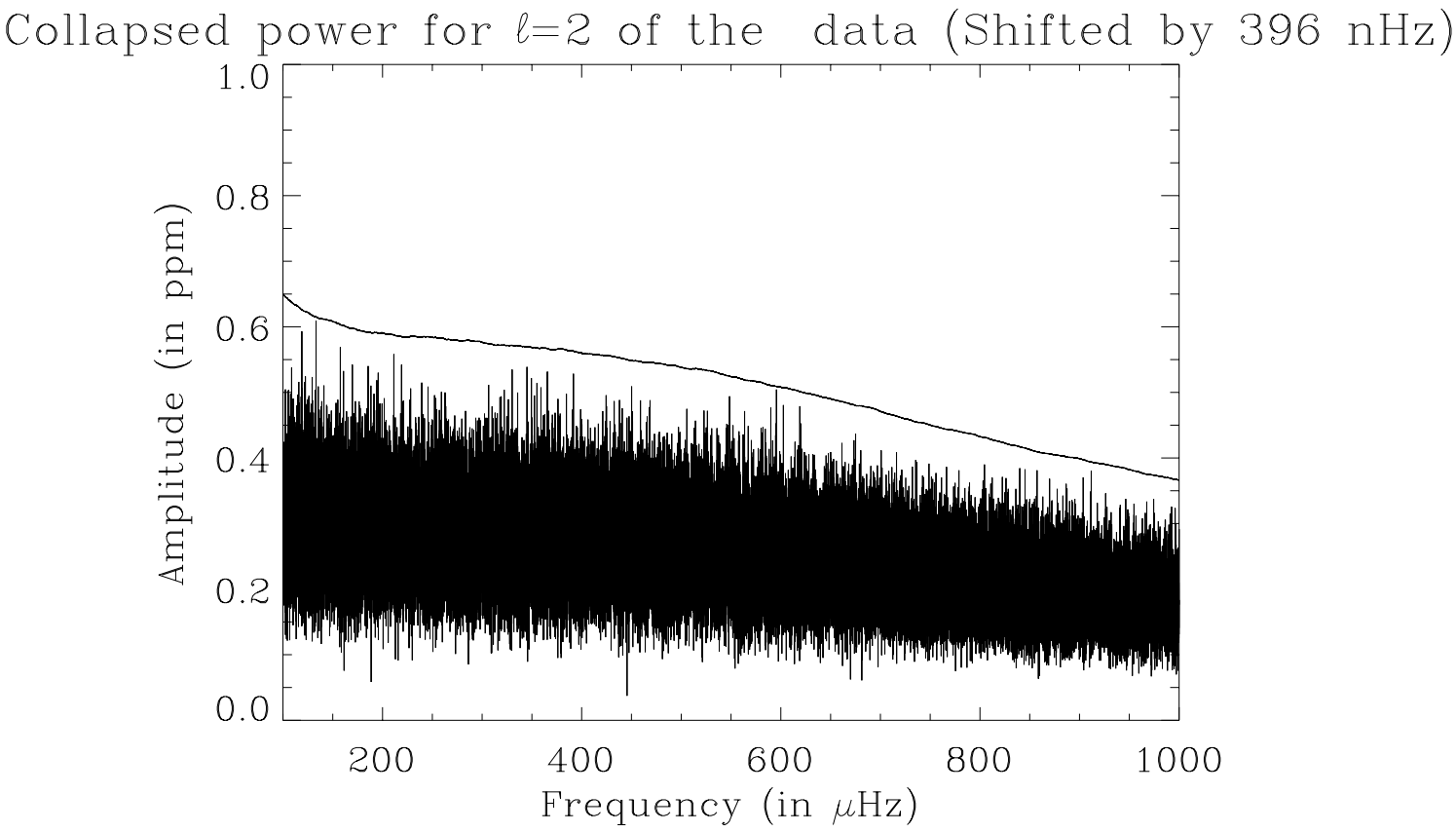

Fig. 7.— LOI collapsed spectra for $l = 2$. The continuous line gives the 0.1 probability limit that a peak be due to noise in a 70 μHz bandwidth. In the power spectrum, this level is about 7.9 σ, e.g. about $\sqrt{7.9}$ in the amplitude spectrum; this level is to be compared with the level of 10.8 that would have been obtained with a single power spectrum

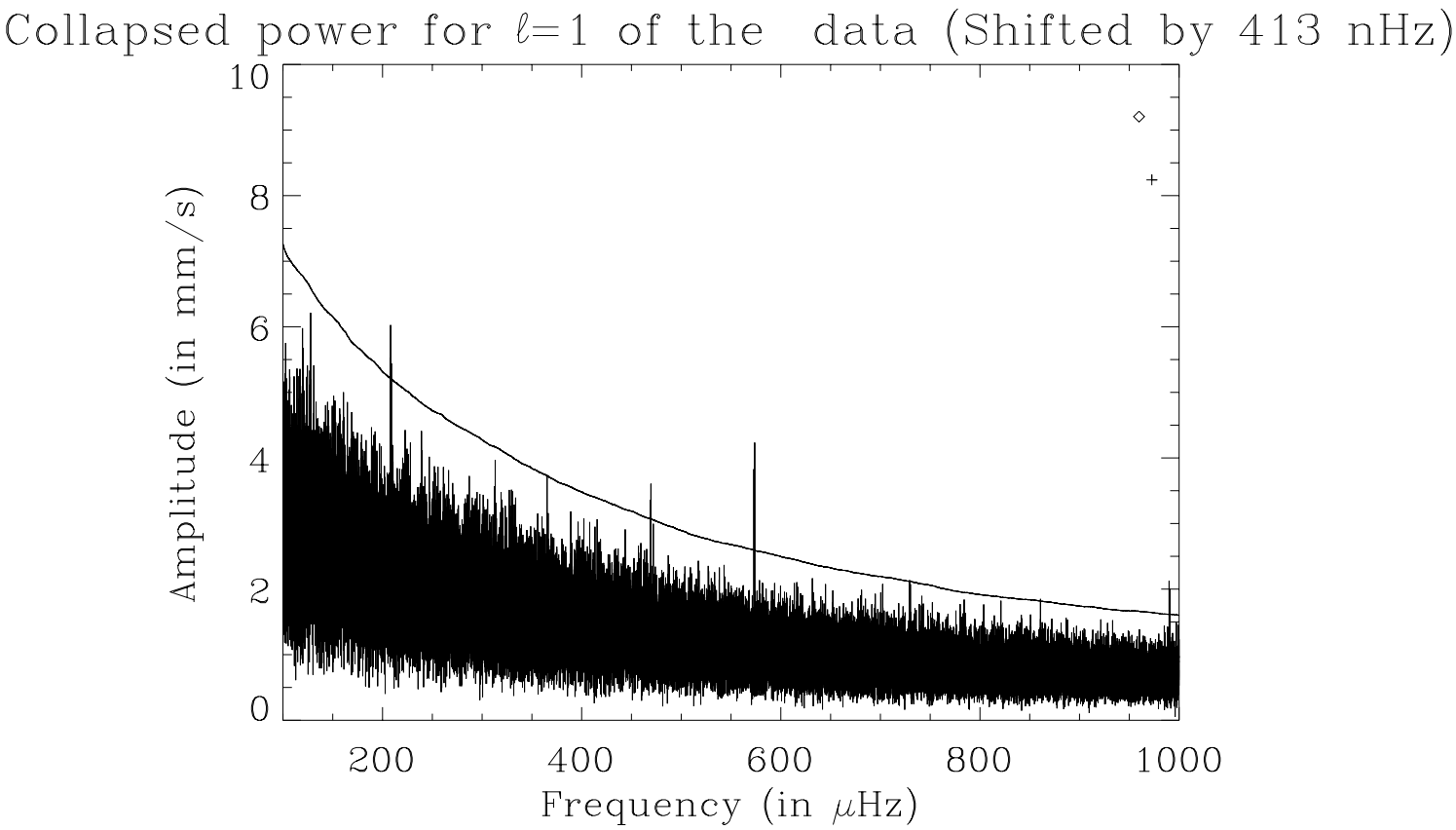

Fig. 8.— SOI/MDI collapsed spectra for $l = 1$. The continuous line gives the 0.1 probability limit that a peak be due to noise in a 70 μHz bandwidth. In the power spectrum, this level is about 10.5 σ, e.g. about $\sqrt{10.5}$ in the amplitude spectrum; this level is to be compared with the level of 10.8 that would have been obtained with a single power spectrum. Peaks above the lines!

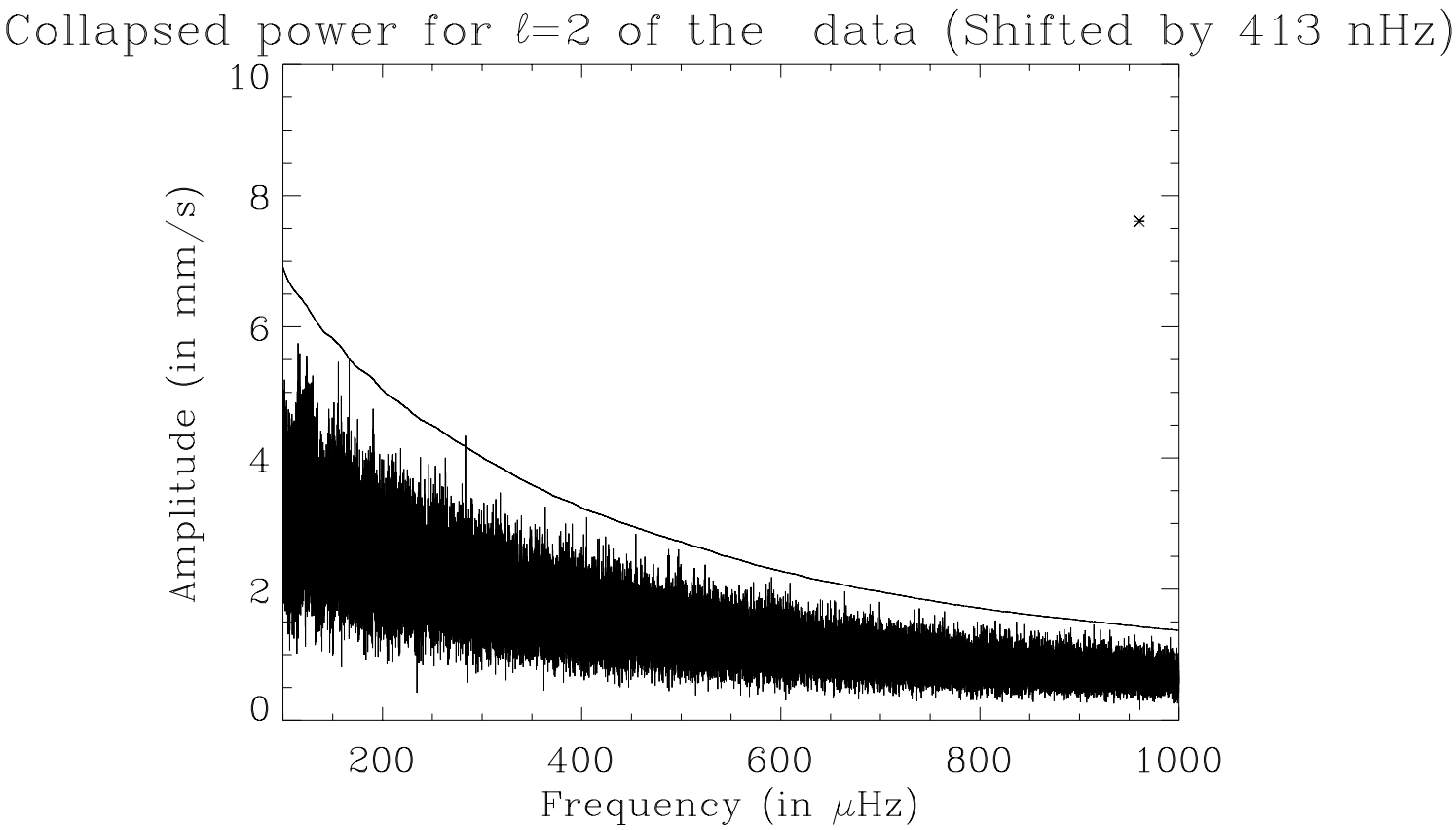

Fig. 9.— SOI/MDI collapsed spectra for $l = 2$. The continuous line gives the 0.1 probability limit that a peak be due to noise in a 70 μHz bandwidth. In the power spectrum, this level is about 7.9 σ, e.g. about $\sqrt{7.9}$ in the amplitude spectrum. this level is to be compared with the level of 10.8 that would have been obtained with a single power spectru. Peaks above the lines!

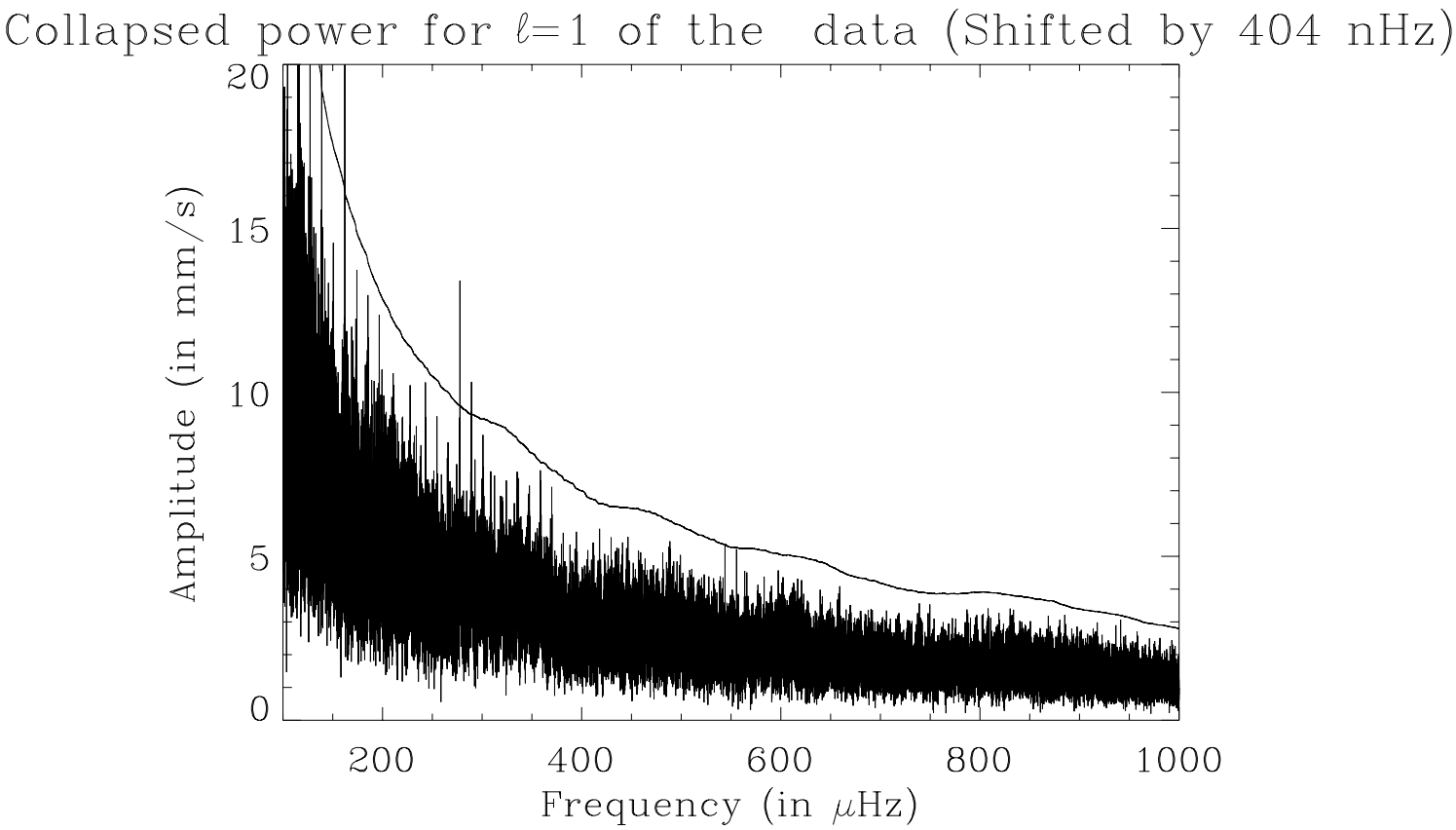

Fig. 10.— GONG collapsed spectra for $l = 1$. The continuous line gives the 0.1 probability limit that a peak be due to noise in a 70 μHz bandwidth. In the power spectrum, this level is about 10.3 σ, e.g. about $\sqrt{10.3}$ in the amplitude spectrum; this level is to be compared with the level of 10.37 that would have been obtained with a single power spectrum. Peaks above the lines!

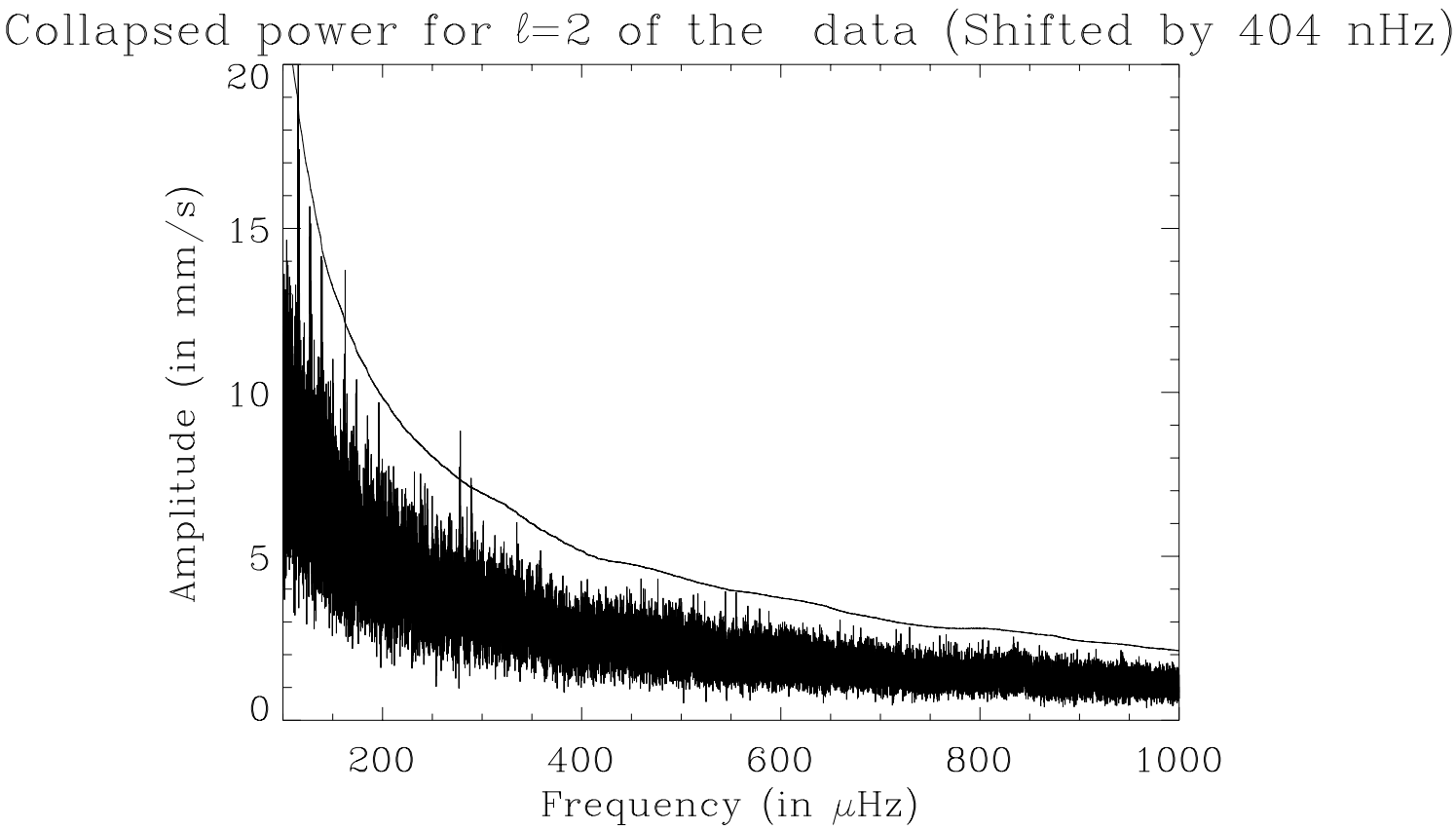

Fig. 11.— GONG collapsed spectra for $l = 2$. The continuous line gives the 0.1 probability limit that a peak be due to noise in a 70 μHz bandwidth. In the power spectrum, this level is about 7.7 σ, e.g. about $\sqrt{7.7}$ in the amplitude spectrum. this level is to be compared with the level of 10.37 that would have been obtained with a single power spectru. Peaks above the lines!

where $\mathbf{f}^X(\lambda)$, $\mathbf{f}^{Y,X}(\lambda)$ and $\mathbf{f}^{X,Y}(\lambda)$ are the power and cross spectral density functions of $\mathbf{X}(t)$ and $Y(t)$ Koopmans 1974.**WF: we need also the coherence to define the signal-to-noise, it is part of the above equation**

The *total coherence* squared $\rho^2(\lambda)$ of $Y(t)$ with $\mathbf{X}(t)$ can be calculated from the $(p \times 1)$-dimensional *matrix complex coherence*

$$\gamma(\lambda) = \frac{\mathbf{f}^X(\lambda)^{-\frac{1}{2}}\mathbf{f}^{X,Y}(\lambda)}{f^Y(\lambda)^{\frac{1}{2}}} \tag{6}$$

where $\mathbf{A}^{-\frac{1}{2}}$ denotes the square root of the inverse of the matrix $\mathbf{A}$, by

$$\rho^2(\lambda) = \gamma(\lambda)^*\gamma(\lambda) = \frac{\mathbf{f}^{Y,X}(\lambda)\mathbf{f}^X(\lambda)^{-1}\mathbf{f}^{X,Y}(\lambda)}{f^Y(\lambda)}. \tag{7}$$

3.4.1. Application to VIRGO data

We applied *MSRA* to the time series of total solar irradiance (TSI) measured by the PMO6 radiometer and the three spectral channels of the sunphotometer (SPM) within VIRGO. We set $Y(t)$ to the TSI time series and $\mathbf{X}(t)$ to the three spectral time series and calculate the corresponding spectral density functions $f^{\mathrm{PMO6}}(\lambda)$ and $f^j(\lambda)$ (j = red, green, blue). From the *smoothed* density functions we calculate the transfer functions $B_j(\lambda)$, according to Eq. 5. Smoothing is necessary because otherwise the individual frequency bins of the density functions are independent of each other and the coherence would always be unity. The total coherence squared in the g-mode range is about 0.8. This means that 80% of the variance of TSI (power in the spectrum) can be explained by the time series of the red, green and blue channels. We use this to reduce the coherent solar noise, which is mainly due to convection near the surface, by subtracting the filtered red, green and blue Fourier spectra from the TSI Fourier spectrum. The remaining spectrum is due to instrumental noise and the g modes. The smoothing of the spectra has to run over certain number of frequency bins which has to be sufficiently large to achieve a certain confidence level, but also small enough to allow the power of a possible g mode to be of similar level as the remaining noise power. We applied a boxcar running mean of 101 bins $\simeq$ 1.4 μHz width. **WF: CF believes that the following may not be a very good argument: "...so the possible 'disturbance' of the noise spectrum by a resonant mode contributes with only 1% to the mean", but will also be much smaller than the remaining noise of 20%, may-be 11 bins would be better, how big was the amplitude of the simulated g mode?**.

With the transfer functions $B_j(\lambda)$ (j = red, green, blue) according to Eq. 5 and $f^{\mathrm{PMO6-V}}(\lambda)$ the original, not smoothed, TSI spectrum, the noise reduced TSI spectrum $\widetilde{f}^{\mathrm{PMO6}}(\lambda)$ can be calculated according to

$$\widetilde{f}^{\mathrm{PMO6}}(\lambda) = f^{\mathrm{PMO6}}(\lambda) - \sum_{j=r,g,b} B_j(\lambda) f^j(\lambda)$$

where $f^j(\lambda)$ are the original, not smoothed, Fourier spectra of TSI and the red, green and blue channels of the SPM, respectively.

In the multivariate regression residuum $\widetilde{f}^{\mathrm{PMO6}}(\lambda)$ 2 out of 10 artificial modes were detected (cf. sect. 3.2.2).

4. Discussion

Here we compare our results with recent theoretical g-mode amplitude from Andersen, Kumar,... and also with recent claims by Gabriel et al without mentioning GOLF (BA and/or CF). We also need to touch upon intensity prediction in order to be able to make our intensity limit understood

5. Conclusion

Restate what we have (TA).

SOHO is a mission of international collaboration between ESA and NASA. BiSON is funded by the UK Particle Physics and Astronomy Research Council (PPARC). We thank all members of the BiSON team in Birmingham, and our hosts at each of the BiSON sites. WJC acknowledges the support of an ESA Internal Fellowship.

REFERENCES

Anklin M., Fröhlich C., Finsterle W., Crommelynck D. A., Dewitte S. 1998, Metrologia, 35, 686

Appourchaux T. 1998, in S. Korzenik, A. Wilson (eds.), Structure and Dynamics of the Interior of the Sun and Sun-like Stars, ESA SP-418, ESA Publications Division, Noordwijk, The Netherlands, p. 37

Appourchaux T., Andersen B., Chaplin W., Elsworth Y., Finsterle W., Fröhlich C., Gough D., Hoeksema J. T., Isaak G., Kosovichev A., Provost J., Scherrer P., Sekii T., Toutain T. 1998a, in S. Korzenik, A. Wilson (eds.), Structure and Dynamics of the Interior of the Sun and Sun-like Stars, ESA SP-418, ESA Publications Division, Noordwijk, The Netherlands, p. 95

Appourchaux T., Andersen B., Fröhlich C., Jimenez A., Telljohann U., Wehrli C. 1997, Sol. Phys., 170, 27

Appourchaux T., Andersen B. N. 1990, Sol. Phys., 128, 91

Appourchaux T., Gizon L., Rabello-Soares M. C. 1998b, A&AS, 132, 107

Christensen-Dalsgaard J. 1998, in S. Korzenik, A. Wilson (eds.), Structure and Dynamics of the Interior of the Sun and Sun-like Stars, ESA SP-418, ESA Publications Division, Noordwijk, The Netherlands, p. 17

Christensen-Dalsgaard J., Däppen W., Ajukov S., Anderson E., Antia H., Basu S., Baturin V., Berthomieu G., Chaboyer B., Chitre S., Cox A., Demarque P., Donatowicz J., Dziembowski W., Gabriel M., Gough D., Guenther D., Guzik J., Harvey J., Hill F., Houdek G., Iglesias C., Kosovichev A., Leibacher J., Morel P., Proffitt C., Provost J., Reiter J., Rhodes, Jr. E., Rogers F., Roxburgh I., Thompson M., Ulrich R. 1996, Science, 272, 1286

Delache P., Scherrer P. H. 1983, Nature, 306, 651

Fröhlich C., Andersen B. N. 1995, in J. T. Hoeksema, V. Domingo, B. Fleck, B. Patrick (eds.), Forth SOHO Workshop: Helioseismology (Invited Reviews), ESA-SP-376, Noordwijk NL, p. 413

Fröhlich C., Delache P. 1984, in R. K. Ulrich, J. Harvey, E. J. Rhodes, J. Toomre (eds.), Solar Seismology from Space, JPL Publ.84-84, Pasadena, p. 183

Fröhlich C., Romero J., Roth H., Wehrli C., Andersen B. N., Appourchaux T., Domingo V., Telljohann U., Berthomieu G., Delache P., Provost J., Toutain T., Crommelynck D. A., Chevalier A., Fichot A., Dappen W., Gough D., Hoeksema T., Jimenez A., Gomez M. F., Herreros J. M., Cortès T. R., Jones A. R., Pap J. M., Willson R. C. 1995, Sol. Phys., 162, 101

Hill F., Stark P., Stebbins R., Anderson E., Antia H., Brown T., Duvall, Jr. T., Haber D., Harvey J., Hathaway D., Howe R., Hubbard R., Jones H., Kennedy J., Korzennik S., Kosovichev A., Leibacher J., Libbrecht K., Pintar J., Rhodes, Jr. E., Schou, J. Thompson M., Tomczyk S., Toner C., Toussaint R., Williams W. 1996, Science, 272, 1292

Hoeksema J., Bush R., Mathur D., Morrison M., Scherrer P. 1998, IAU Symposia, 181, 31

Hoogeveen G. W., Riley P. 1998, Sol. Phys., 179, 167

Koopmans L. 1974, The Spectral Analysis of Time Series, Academic Press, Inc., London, GB

Kotov V. A., Severnyi A. B., Tsap T. T. 1978, MNRAS, 183, 61

Neckel H., Labs D. 1994, Sol. Phys., 153, 91

Rabello-Soares M. C., Appourchaux T. 1999, A&A, 345, 1027

Scherrer P. H. 1984, in Solar Seismology from Space, JPL Publication 84-84, p. 173

Scherrer P. H., Wilcox J. M., Kotov V. A., Severny A. B., Tsap T. T. 1979, Nature, 277, 635

Thomson D. J., Maclennan C. G., Lanzerotti L. J. 1995, Nature, 376, 139

Toutain T., Kosovichev A. 1998, in S. Korzenik, A. Wilson (eds.), Structure and Dynamics of the Interior of the Sun and Sun-like Stars, ESA SP-418, ESA Publications Division, Noordwijk, The Netherlands, p. 349